A Numerical Framework for Airfoil Gust Response and Active Pitch Control

Ernest Grau Lozano
ISAE-SUPAERO, Université de Toulouse, 31055 Toulouse, France
Universitat Politècnica de València, 46022 Valencia, Spain

Because of their small size, micro air vehicles (MAV) are susceptible to be destabilised by wind gusts, especially in urban environments. The likely increasing use of these unmanned vehicles in cities implies that understanding the dynamics of a MAV in a gust encounter and studying control laws that can swiftly return it to its original position is a requirement for the urban airspace organisation and its use in activities such as environmental research. By means of 2D URANS simulations in StarCCM+ for Re ∼ 30000, the dynamics of a MAV represented by an airfoil associated with a structural model are simulated for gusts in the frontal and transverse direction. A proportional pitch controller is implemented within the framework and tested for different gust cases, showing that this strategy is only suitable for vehicles that can support high pitch rates. Both the free and controlled responses of the 2D airfoil reproduce trends found in previous experimental work for flat plates and Re ∼ 40000. An attempt to separate the lift in its contributions for frontal gusts is performed. For vertical velocity disturbances, the lift coefficient is linked to the variation in the effective angle of attack. The lift coefficient variation during a gust encounter can indeed be approximated as $2\pi \times \alpha_{\text{eff}}$.

Nomenclature

A_{p}	=	pitch motion amplitude
A_{pl}	=	plunge motion amplitude, m
c	=	airfoil chord, m
C_L	=	lift coefficient
C_L^a	=	approximation of the α_{eff} contribution to C_L
C_L^b	=	approximation of the gust contribution to C_L
C_{L0}	=	lift coefficient at null angle of attack
f_g	=	gust velocity profile frequency, Hz
f_{p}	=	pitch motion frequency, Hz
f_{p}	=	plunge motion frequency, Hz
F	=	force, N
F_f	=	fluid force, N
g	=	gravitational acceleration, m s^{-2}
GR	=	gust ratio
k_y	=	vertical spring constant, N m^{-1}
k_θ	=	torsional spring constant, Ndeg^{-1}
K	=	proportional controller constant, N m^2
L	=	lift, , N
L^a	=	approx. of the α_{eff} contribution to the lift, N
L^b	=	approx. of the gust contribution to the lift, N
m	=	airfoil mass, kg
M	=	moment, N m
M_0	=	fixed aerodynamic moment, N m
M_f	=	fluid moment, N m
$M_{\text{controller}}$	=	moment introduced by the controller, N m
P	=	static pressure, Pa
t	=	time, s
t^*	=	convective time
t_g	=	gust start time, s
U_∞	=	freestream velocity, m s^{-1}
v_c	=	1-cos velocity profile, m s^{-1}
v_g	=	maximum gust velocity, m s^{-1}
v_s	=	sine-squared velocity profile, m s^{-1}
W	=	transverse gust width, m
x	=	horizontal position coordinate, m
x_0	=	left domain wall horizontal distance, m
x_w	=	transverse gust right side position, m
x_{CM}	=	airfoil centre of mass position, m
y	=	vertical position coordinate, m
$\dot{y}$	=	vertical position rate, m s^{-1}
y_0	=	reference vertical position, m
y^+	=	dimensionless wall distance
α	=	pitch angle
α_0	=	initial pitch motion incidence
α_{eff}	=	effective angle of attack
α_{pl}	=	vertical-velocity-induced angle of attack
α_{gust}	=	gust-induced angle of attack
μ	=	dynamic viscosity, Pa s
ρ	=	density, kg m^{-3}
ϕ_0	=	transverse gust phase
Φ	=	plunge motion phase

I. Introduction

AEROSPACE vehicles, turbines and turbomachines are usually subjected to combined pitch and plunge motion. The combination of rotational and vertical movement, that can appear as a response to wind gusts, affects the effective angle of attack and is behind complex phenomena like dynamic stall or aerodynamic hysteresis. This is why the study of situations where these complex dynamics are present is of interest.

The next decade is likely to witness a considerable rise in the use of micro air vehicles (MAV) in cities as part of the ecological transition, revolutionising several aspects such as mobility or environmental data gathering and research, and so making it essential to examine the different aspects involved. These vehicles are particularly susceptible to be destabilised by gusts which loads are proportionally higher relative to their small size, causing high-amplitude oscillatory horizontal displacements and changes of incidence, i.e. a pitch-plunge movement. This is especially meaningful in urban environments, characterised by sudden crosswinds and turbulent drafts [1]. A stable flight

altitude may be required by environmental research and for urban airspace organisation. In order for these vehicles to be stable in an urban environment, it is necessary to study control laws to dampen the response of MAVs to gusts.

In terms of wind gusts modelling, Golubev and Visbal proposed three canonical gust models for urban environments, namely the sharp-edge gust, the time-harmonic and the Taylor vortex models [1]. Nevertheless, studies commonly make the distinction between frontal, transverse and vortex gusts.

Frontal gusts are a variation of the velocity in the flight direction, and so affecting the Reynolds number and possibly affecting the stall angle. Transverse gusts cause fluctuations in the flight-normal direction, inducing a change in the effective angle of attack. Sharp-edge and time-harmonic gusts can be either frontal or transverse gusts. Vortex gusts cause fluctuation in both directions.

Transverse and frontal gust response studies often use typical discrete gust models like the 1-cos gust profile [2–4] to simulate a smoother gust appearance, or a step change (or sharp-edge profile) [2, 4] to simulate a more sudden change. Other works also use the Mexican gust [3] or a sine-squared [5–7] profile, similar to the 1-cos gust.

Regarding gust-airfoil simulation, two main approaches can be found: analytical models and numerical (CFD) simulations. Due to the difference in computational cost and fidelity level, each technique shall be used depending on the objective of the study. In both cases, most studies for different applications use a 2D airfoil.

Analytical models, since they require a lower computational effort, are usually sufficient for most cases, like the analysis of the off-design conditions of an airplane or preliminar aeroelastic analysis. They are usually chosen to analyse complex control laws considering noise, delay and actuator dynamics [8] or algorithms to find optimal control laws [9]. Some examples of analytic models are the Wagner and the Thedorsen models used in [10] or the modified Goman-Khrabrov model developed in [9].

On the other hand, CFD simulation studies usually focus on active flow control with techniques like suction or blowing [2, 4] or on the comparison to analytic models [3, 10] or experimental results [7]. A 2D URANS setup with k-ω SST turbulence model and the mesh velocity technique for transverse gusts [2–4] is commonly used. Sometimes, 3D simulations are also used to simulate wings or flat plates [7]. Morphing and overset mesh techniques can also be found [11].

Analytical models usually account for pitch angle variation and vertical displacement. In numerical simulations these quantities are not commonly simulated: the fluid forces and moments are computed over a fixed airfoil. These types of research study the aerodynamics of gust encounters, focusing on vortex generation or on the evolution of the lift coefficient with time or the effective angle of attack, but do not take into account airfoil dynamics. However, Gillebaart et al. computed the vertical displacement and angle of attack variation in a CFD simulation by coupling the fluid-airfoil dynamics with an aeroelastic model [3].

For fixed airfoil simulations, the field velocity method is a popular tool to reproduce the transverse gust disturbance. This method applies the gust velocity profile to the grid points at every time step, capturing the effect of the gust on the wing but not the effect of the wing on the gust [7]. The wing-gust coupling is accounted for in recent studies by adding a source term to the field velocity method [12], developing the Split Velocity Method.

These methods have advantages over applying the gust at the boundary conditions. This last approach requires finer grids —leading to higher computational cost— so that the gust disturbance is not dissipated as it travels through the domain to the airfoil [12].

A fixed airfoil setup makes the results more comparable with experiments, where the studied aerodynamic surface is fixed. The facility for transverse gust encounter of the University of Maryland used in [6, 7, 13] is a good example. Works in this experimental setup employ rails to move the wing towards the stationary transverse gust flow velocity field generated.

Apart from the complex flux control techniques, control laws acting on the pitch [5, 9] and flap position [3, 8, 11] are used to maintain a stable lift. When analytic and CFD models were compared in [3], it was shown that even if there was a good agreement in the airfoil dynamic response and a similar reduction in vertical displacement, there were significant differences in the pitching angle and moment. The employed control law was a simple PD controller that used the vertical velocity and acceleration as input to regulate the flap position.

Sedky et al. studied the aerodynamics of lift regulation with a proportional feedback gain over a flat plate [5]. The pitching control strategy was applied following the results of Xu and Lagor, who applied a gradient descent algorithm to find an optimal pitching control law [9]. That law was compared to a simple proportional feedback law, using the lift coefficient as input, which showed similar results. Sedky et al. suggested that these kind of simple proportional laws may only be suitable for vehicles that can achieve high pitch rates, like it is the case of a MAV.

The aim of the present work is to create a numerical framework to study the dynamics of a MAV subjected to wind gusts and to apply control laws to stabilise its response.

Numerical simulations are an advantageous tool to understand the physics of the airfoil response to gusts and control laws. Whereas CFD can be computationally expensive, it allows us to capture with fidelity the fluid structures, which is especially useful when we have significant pitch-plunge rates.

A simple pitch control law strategy is applied in this article by means of 2D simulations of an airfoil (representing a MAV) subjected to both frontal and transverse wind gusts. The airfoil response and pitch control simulations were performed using StarCCM+ v16.02. By means of a fluid-body interaction solver, the software computes and applies the movement of the air vehicle in every time step, enabling to simulate the airfoil dynamics and the airfoil-gust flow coupling. This work intends to be a first step to understand the actual MAV dynamics in gust encounters via CFD. Being a preliminary study, we perform URANS simulations with gusts generated with a far-field boundary condition approach.

This paper is organized as follows: The methodology, including the simulations setup and the control laws used, is outlined in Sec. II. The mesh is validated in Sec. III. The airfoil gust response and controller effect are discussed in Sec. IV, and the conclusions of the study are drawn in Sec. V.

II. Numerical methods

A. URANS solver

The software used for this work was STAR-CCM+ v16.02, a commercially available multidisciplinary solution that uses the finite-volume method to discretise the Navier-Stokes equation. We used the implicit unsteady solver with second order time discretisation. Regarding the turbulent scheme, a 2D URANS setup with k–ω SST turbulence model is implemented. As seen in Sec. I, this is a common configuration in numerical research for airfoil gust response. This scheme was complemented with the one-equation correlation-based Gamma transition model. Since no compressible phenomena are expected, the solver is pressure-based and segregated.

B. DFBI solver and airfoil dynamics

The airfoil dynamics in response to gusts are computed using Dynamic Fluid Body Interaction (DFBI) module available in STAR-CCM+. The calculated motion is applied by means of the moving domain technique, i.e., by applying movement to the

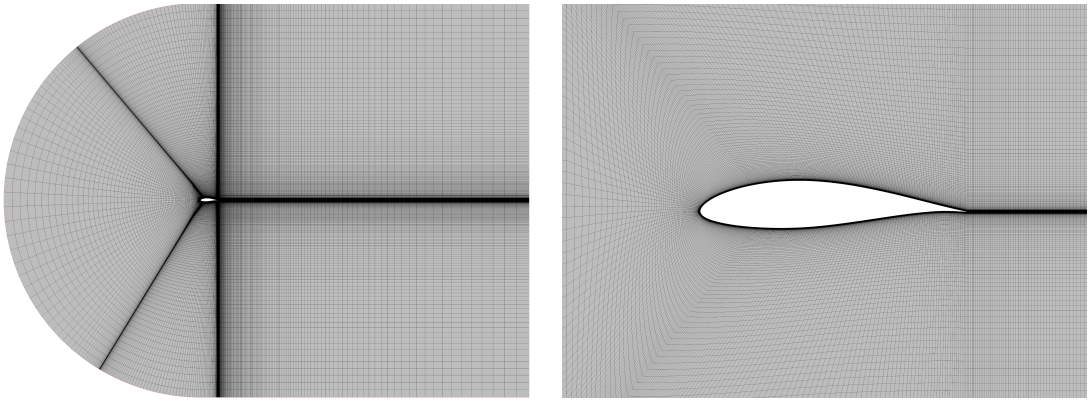

Fig. 1 General and detailed view of the 2D mesh.

whole mesh. This technique was found to be computationally less expensive than using an overset mesh for the simulation of the combined pitch-plunge motion [14].

Using two solvers, the 6-DOF solver and the 6-DOF Motion solver, the DFBI resolves the airfoil motion. The first solver computes the forces and moments acting on the airfoil and moves the center of mass of the body by solving the governing equations of free motion.

The 6-DOF solver uses a trapezoidal scheme with second-order accuracy for temporal integration (independent of the order of accuracy of the implicit unsteady solver). The second solver shifts the vertices of the grid in accordance with the motion of the body computed by the first.

The DFBI module allows to define a 2D rigid body with free motion. In addition to the fluid ones, other forces and moments acting on the airfoil can be defined. We add forces and moments following a structural model based on a typical aeroelastic model based on a vertical and torsional spring.

Assuming the MAV (represented by the airfoil) is stable, it should maintain the same flight altitude during the simulation in cruise and return to this position naturally after a wind gust disturbance, without the need of a controller. To ensure these two conditions, the model is composed of a fixed moment representing the horizontal stabiliser to ensure cruise stability, and two springs at the centre of mass (one vertical and one torsional) that bring the airfoil to the equilibrium position. Eventually, the moment introduced by the controller is also introduced.

Equations (1) and (2) are the complete equations of motion that will be solved by the 6-DOF solver.

$$m\frac{\mathrm{d}v}{\mathrm{d}t} = \Sigma F = F_f - mg - k_y y \tag{1}$$

$$I\frac{\delta\dot{\alpha}}{\delta t} = \Sigma M = M_f + M_0 - k_\theta \alpha + M_{\text{controller}} \tag{2}$$

Preliminary simulations were carried out to find the mass m and the moment M_0 associated with the airfoil so that the it is stable in cruise conditions. The DFBI module also requires the position of the centre of mass and the moment of inertia with respect to a coordinate system, that we situated at the leading edge. These quantities, together with the rest of parameters of the structural model can be found in Table 1.

C. Simulation conditions

The studied MAV is represented by the airfoil of chord $c = 0.25\,\text{m}$ used by Akhlaghi et al. [15]. The computational domain is a C-type domain, with the front and back boundaries separated, respectively, 12 and 20 chord lengths from the leading edge.

The fluid around the airfoil is air with density $\rho = 1.004\,86\,\text{kg}\,\text{m}^{-3}$, dynamic viscosity $\mu = 1.825 \times 10^{-5}\,\text{Pa}\,\text{s}$ and static pressure $P = 84\,500\,\text{Pa}$, to replicate the conditions of the experimental study of the pitch-plunge motion in [15].

Table 1 Parameters of the structural model.

Parameter	Symbol	Value
Airfoil mass	m	$1.976\,\text{kg}$
Fixed moment	M_0	$0.6349\,\text{N}\,\text{m}$
Vertical spring constant	k_y	$12.5\,\text{N}\,\text{m}^{-1}$
Torsional spring moment	k_θ	$1\,\text{N}\,\text{m}\,\text{rad}^{-1}$
Moment of inertia	I	$0.05\,\text{kg}\,\text{m}^{-2}$
Centre of mass	x_{CM}	$0.0875\,\text{m}$

The airfoil moves at a cruise speed of $U_\infty = 20\,\text{m}\,\text{s}^{-1}$. The simulation is therefore carried out at a transitional Reynolds number of 2.75×10^5. For this reason, we applied a URANS k–ω SST turbulence scheme complemented with a Gamma-Re transition model.

Regarding the boundary conditions, the inlet and the domain walls are set as velocity inlet, except for the rear wall that is set as pressure outlet of 0 Pa relative pressure. The velocity in the boundary conditions is applied by its components. The gust treatment by the boundary conditions is outlined in Sec. II.E.

D. Mesh resolution and time independence

The mesh used in the present study was defined in the study by Kesarwani, Sundararaman, Jain, and Galal [14]. The 2D C-type structured grid is composed of 115k cells. The front and back boundaries are separated, respectively, 12 and 20 chord lengths from the leading edge. The first cell height of $4\times10^{-5}\,\text{m}$ is set to obtain a $y^+ \sim 1$. The grid resolution was obtained with a mesh independence study. A time independence analysis was also performed, obtaining a time step of $0.001\,938\,\text{s}$.

The resulting mesh, which can be seen in Fig. 1, was validated for pitch-plunge motions at low incidence. In Sec. III, the validity of the grid for high angles of attack is discussed.

E. Gust definition and treatment

In this project, we will differentiate between vertical and frontal gusts. On the one hand, vertical perturbations are characterised by their intensity and duration. The associated velocity profile is only a function of time, so the vertical velocity introduced at a given time is the same at all the boundary points. On the other hand, frontal gusts are characterised by their intensity and width. The velocity profile is the equation of a discrete wave that moves towards the airfoil at velocity U_∞. The profile is thus both a function of time and space.

For simplicity, we performed simulations using a gusts with a 1-cos and a sine-squared profile only. The velocity profiles are defined as follows:

$$v_c(t) = \begin{cases} \dfrac{v_g}{2}(1 - \cos(2\pi f_g(t - t_g))) & \text{if } 0 < t - t_g < 1/f_g \\ 0 & \text{otherwise} \end{cases}$$

$$v_s(t,x) = \begin{cases} \frac{v_g}{2}\sin^2\left(\frac{\pi}{W}(x - U_\infty t) + \phi_0\right) & \text{if } 0 < x_w - x < W \\ 0 & \text{otherwise} \end{cases}$$

Where $x_w = x_0 + U_\infty t$ is the position of the right side of the wave and ϕ_0 is the phase that ensures $v_g(t, x_w) = 0$.

The gust ratio is a measure of the intensity of the gust and is defined as $GR = v_g/U_\infty$.

These velocity profiles are applied as perturbations of the boundary conditions. Three different case groups were studied: frontal 1-cos gusts, vertical 1-cos gusts and transverse sine-squared gusts. In the a case with a frontal gust, the velocity profile is added to the velocity in the streamwise directon U_∞. For transverse gusts, the velocity profile represents the velocity in the streamwise normal direction.

F. Controller

The present work implements a simple proportional pitching controller, that applies an angular acceleration to the airfoil proportional to the vertical displacement, taking as reference position $y_0 = 0$ m. This was implemented in the 6-DOF solver by adding a moment proportional to the vertical translation. This controller is described in Eq. (3).

$$M_{\text{controller}} = K(y - y_0) = Ky \tag{3}$$

III. Mesh Validation

The used mesh was developed by Kesarwani, Sundararaman, Jain, and Galal [14] to reproduce pitch-plunge motions at effective angles of attack between −5° and 5°. The mesh needs thus to be validated to confirm that it can correctly simulate fluid behavior at higher effective angles of attack in STAR-CCM+. To do so, we impose the pitch-plunge motions from the work of Akhlaghi et al. and compare the lift coefficient hysteresis loops.

Pitch-plunge motion with amplitudes of 2° and 5° is applied on a profile at different initial incidences, obtaining a range of curves ranging from −5° to 20° of effective angle of attack. The equations of motion are the following:

$$\alpha(t) = \alpha_0 + A_\text{p}\sin(2\pi f_\text{p} t)$$

$$y(t) = A_\text{pl} sin(2\pi f_\text{pl} t + \Phi)$$

Provided $f_\text{p} = f_\text{pl}$, the phase difference defines the two motions studied in [15]: constructive ($\Phi = \pi/3$) and destructive ($\Phi = 3\pi/4$).

The vertical speed induces an angle of attack that has to be added to the pitch motion to obtain the effective angle of attack. The plunge-induced angle of attack can be expressed as:

$$\alpha_\text{pl}(t) = \arctan\left(\frac{-\dot{y}(t)}{U_\infty}\right) = \arctan\left(\frac{2\pi f_\text{pl} A_\text{pl}}{U_\infty}\cos(2\pi f_\text{pl} t + \Phi)\right)$$

Using a time step of 0.001 938 s, we find high levels of noise in the resulting lift coefficient curves. Figure 2 shows the obtained hysteresis loops for the constructive motion for $A_\text{p} = 5°$.

Despite the level of noise, the shape of the curves and the values around which they oscillate seem to be correct. Looking at the evolution of the lift coefficient with time, we detected that the noise starts to appear around 10°. In order to reduce the levels of noise, three strategies were implemented:

- Reduce the time step from 0.001938 to 0.000969 seconds.
- Filter the signal if there are still some levels of noise.
- Average the last four cycles if the resulting filtered signal is not periodic.

The implemented filter is a lowpass FIR filter of cutoff frequency 5 Hz that uses a rectangular window. The order of the filter depends on the levels of noise found in each case.

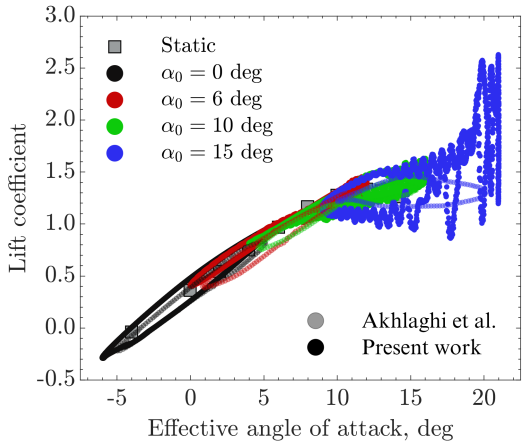

Fig. 2 Lift coefficient hysteresis loop for $\Delta t = 0.001938$ s (Case: constructive, $A_\text{p} = 5°$).

The lift coefficient hysteresis loops obtained after applying these strategies are shown in Fig. 3.

The mesh fails to capture the fluid behaviour for angles greater than 12°. For the high-amplitude motion, the airfoil shows a hysteresis loop compatible with dynamic stall, a phenomenon not found in the experimental study. This effect does not appear for the low-amplitude motions, where the lift is underestimated. For lower angles, although the mesh captures the hysteresis loop shape, the numerical scheme tends to overestimate the lift, with an acceptable level of error.

Significant changes were found in the mean shape of the curves for high angles of attack when halving the time step. The time step was again reduced to confirm the time independence of the results. Figure 4 shows the evolution of the lift coefficient with time computed with the three time steps. We plotted in addition the last of the signals filtered to show the filter functioning. There are still significant differences in the start and at the end of each cycle. Therefore, time independence cannot be ensured, which limits the validity of the used mesh.

The mesh will only be used to only perform simulations where the effective angle of attack is not expected to exceed 12°, given that at this point differences between the experimental and numerical results (and between simulations at different time steps) start being significant. For lower angles, the hysteresis loops show a level of agreement with the experimental results that permits them to be considered as correct.

IV. Results and Discussion

A. Frontal gusts

Frontal gusts affect the stream velocity, which increases or decreases the lift and so modifies the flight altitude of the airfoil. The vertical velocity of the airfoil induces an angle of attack that has to be added to the pitch angle to obtain α_eff:

$$\alpha_\text{eff} = \alpha + \alpha_\text{pl} = \alpha + \arctan\left(\frac{-\dot{y}(t)}{U_\infty}\right)$$

For simplicity, only one case has been studied: a 1-cos gust of $GR = 0.25$ and $f_g = 0.5$ Hz. The airfoil response is analysed for five different control cases varying the K value between 0 (free response) and 30.

The lift coefficient definition in Eq. (4) is used for all the three gust types (frontal, vertical and transverse), with reference velocity U_∞ and not considering the perturbation v_c in frontal gust.

$$C_L = \frac{2L}{\rho U_\infty^2 c} \tag{4}$$

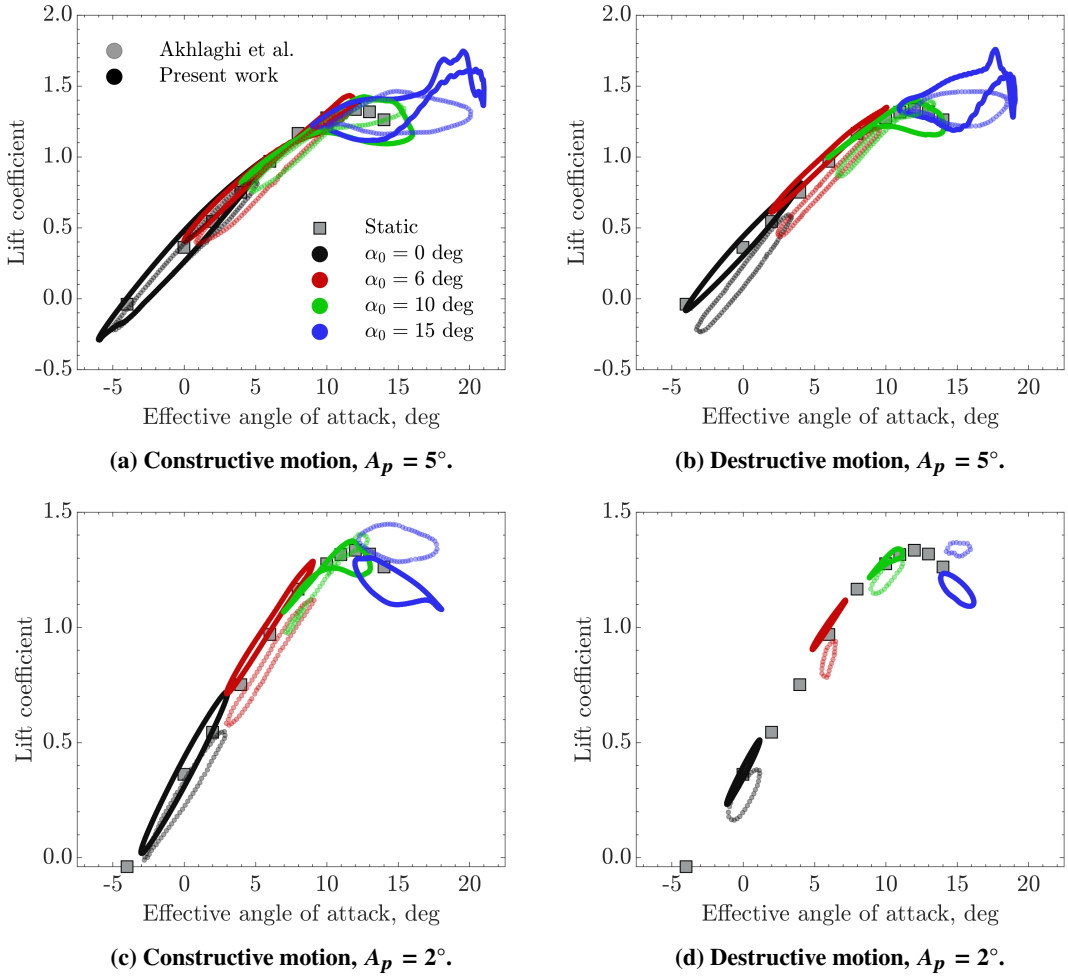

(a) Constructive motion, $A_p = 5°$. **(b) Destructive motion, $A_p = 5°$.**

(c) Constructive motion, $A_p = 2°$. **(d) Destructive motion, $A_p = 2°$.**

Fig. 3 Comparison of the hysteresis curves for combined pitch-plunge motions obtained numerically and the experimental results from Akhlaghi et al. [15].

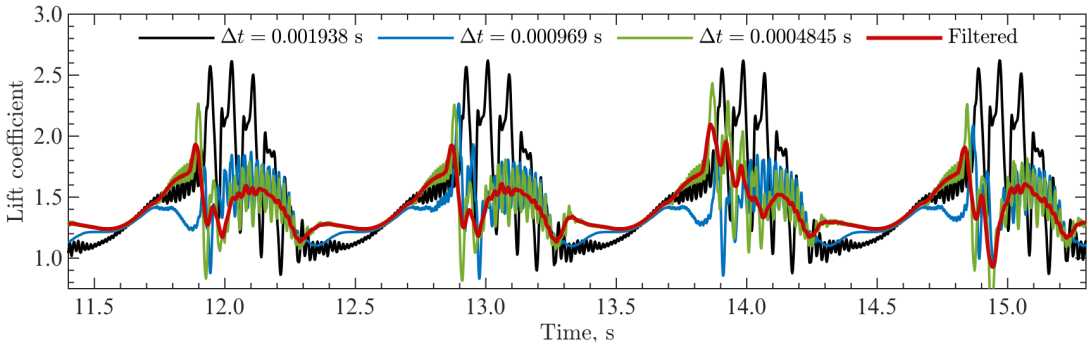

Fig. 4 Lift coefficient evolution with time (constructive, $A_p = 5°$, $\alpha_0 = 15°$) for different time steps and filtered signal.

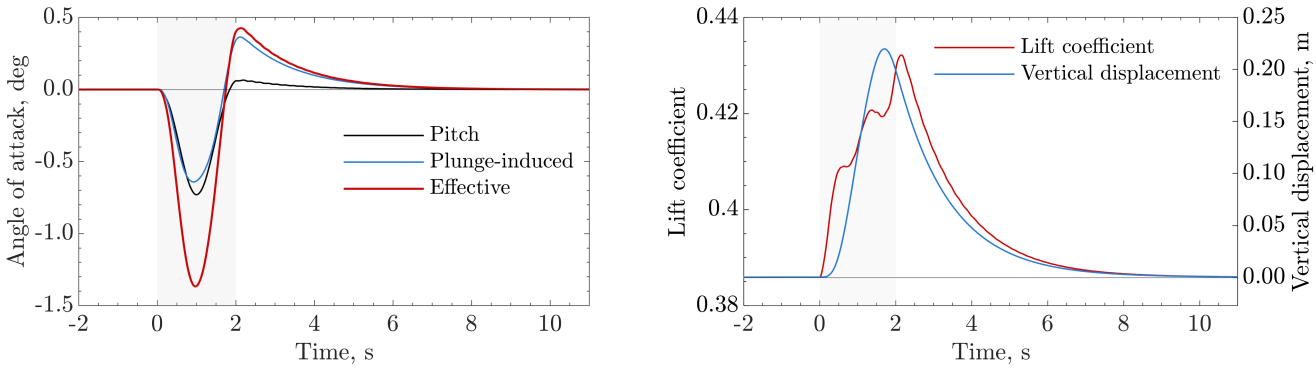

Fig. 5 Airfoil response to a frontal gust of $GR = 0.25$ and $f_g = 0.5$ Hz.

Figure 5 shows the free response to the gust studied. The effect on the effective angle of attack can be observed. As the gust entrains a vertical velocity upwards, it induces a negative angle of attack which contribution is similar to the pitch angle.

Two differentiated stages can be found. In the first one, the airfoil is ascending with a negative effective angle of attack. The vertical velocity increases as the gust intensity increases. When the gust intensity starts decreasing, the upwards force is reduced so the airfoil decelerates and the effective angle of attack decreases until reaching zero. At this point, the maximum altitude is reached, the airfoil starts descending and the second stage begins. This phase is dominated by the plunge motion, being the main contribution to the effective angle of attack. The maximum effective angle of attack is reached just after the gust duration when the descent has started and the downwards vertical velocity is at its highest. This point coincides with the maximum lift coefficient.

To explore the lift components that can produce the lift coefficient curve shape, we define a lift coefficient that takes as reference velocity $U_\infty + v_c$:

$$C_L^a = \frac{2L}{\rho\,(U_\infty + v_c)^2\,c} = C_L \frac{U_\infty^2}{(U_\infty + v_c)^2}$$

From the previous definition, the lift contribution L^a can be deduced:

$$L^a = L \frac{U_\infty^2}{(U_\infty + v_c)^2}$$

Thus, an equivalent formulation of C_L^a with U_∞ as reference velocity is:

$$C_L^a = \frac{2L^a}{\rho U_\infty^2 c}$$

We define the second lift contribution subtracting the effect of the effective angle of attack to the lift: $L^b = L - L^a$. The second lift coefficient contribution is thus:

$$C_L^b = \frac{2L^b}{\rho U_\infty^2 c} = \frac{2\,(L - L^a)}{\rho U_\infty^2 c} = C_L - C_L^a$$

Figure 6 shows the lift coefficient components and the total lift coefficient as defined in Eq. 4. In addition, we plotted an approximation of the lift coefficient produced by the effective angle of attack.

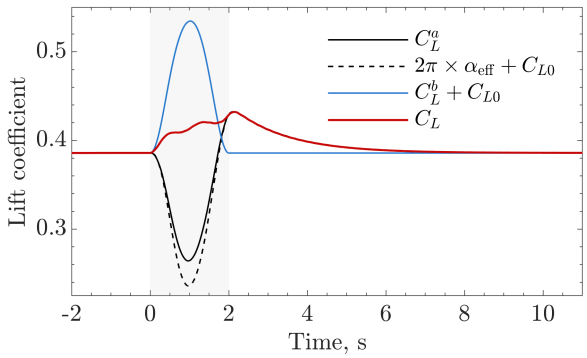

Fig. 6 Approximations to the lift contributions of α_{eff} and v_c in a frontal gust.

From the shape of the curves, it can be deduced what are the magnitudes that influence the lift response. The evolution of L^a matches the evolution of α_{eff}, so it can be deduced that the negative effective angle of attack induces a negative lift. L^b matches the gust duration and is comparable in the velocity profile shape. However, the shape is not completely symmetrical and reaches its maximum at a time higher than half the gust period. We can reckon there the effect of the increase of velocity in the lift. However, the α_{eff}-based lift approximation does not show good agreement with C_L^b within the gust duration. Not being able to observe any fluid phenomena explaining this deviation, we conclude that the effect of the effective angle of attack and of the increase in velocity cannot be completely decoupled. L^a and L^b are, however, an approximation to these contributions that originate the lift curve shape.

Figure 7 shows the airfoil response under the action of the pitch controller for different K values. In both gust cases, the time to reach the initial velocity is highly reduced no matter the controller constant used. The benefit of a high K value lies in the reduction of the maximum displacement.

The controller introduces a pitch moment as the airfoil increases its altitude. This means that the MAV will tend to decrease its pitch angle to reduce the increase in lift due to the increment in frontal velocity. For the controlled response, this strategy reduces the vertical velocity to such an extent that the plunge-induced angle component is a minor component of the effective angle of attack. The pitch represents nearly the entire α_{eff}. Since the effective angle of attack has not varied between for the different values of K, it can be deduced that the proportional controller produces a trade-off between the two α_{eff} components.

B. Vertical gusts

Vertical gusts affect the stream-normal velocity and cause a vertical velocity. Their opposite contributions and the pitch angle are considered to obtain α_{eff}:

$$\alpha_{\text{eff}} = \alpha + \alpha_{\text{pl}} + \alpha_{\text{gust}} = \alpha + \arctan\left(\frac{-\dot{y}(t)}{U_\infty}\right) + \arctan\left(\frac{v_c(t)}{U_\infty}\right)$$

Two gust cases with a 1-cos profile have been studied: a moderate-intensity gust of $GR = 0.25$ and $f_g = 0.5$ Hz and a less intense but shorter gust of $GR = 0.1$ and $f_g = 1$ Hz. The airfoil response is analysed for five different control cases: the free (uncontrolled) response and four controlled responses with K ranging from 5 to 30.

Figure 8 shows the free response to the gust studied. The plunge and gust opposite contributions to the effective angle of attack can be observed.

In both cases, the α_{eff} curve has a characteristic shape with two local maxima with a local minimum in between. This outline is generated by a positive gust-induced profile and a shifted negative plunge-induced with similar sinusoidal shape. The position and value of the extrema are characterised by the intensity and delay of the two main contributions. The pitch curve shape is similar to the α_{eff} curve. Its contribution, however, is much smaller compared to the other two.

The lift coefficient variation shape is similar to the effective angle of attack one, indicating the relation between these two variables.

As for frontal gusts, the vertical displacement divides the gust response in two stages: the ascending phase dominated by the gust-plunge interaction and the descending one dominated by the descending velocity. These two phases do not occur at the same time for the two cases. Even though the maximum height is in both cases reached before the end of the gust, in the second phase the descent starts later and lasts longer (relative to the gust duration).

As expected, a greater gust intensity produces a greater vertical displacement. After the gust effect, a greater displacement produces a greater force in the vertical spring of the structural model, and so getting faster to the equilibrium position. The descending stage is therefore very dependent on the structural model chosen. The model used was employed to perform a preliminary analysis. More complex models representing the air vehicle dynamics better shall be developed and applied so that this stage is representative of its actual behaviour. This simple

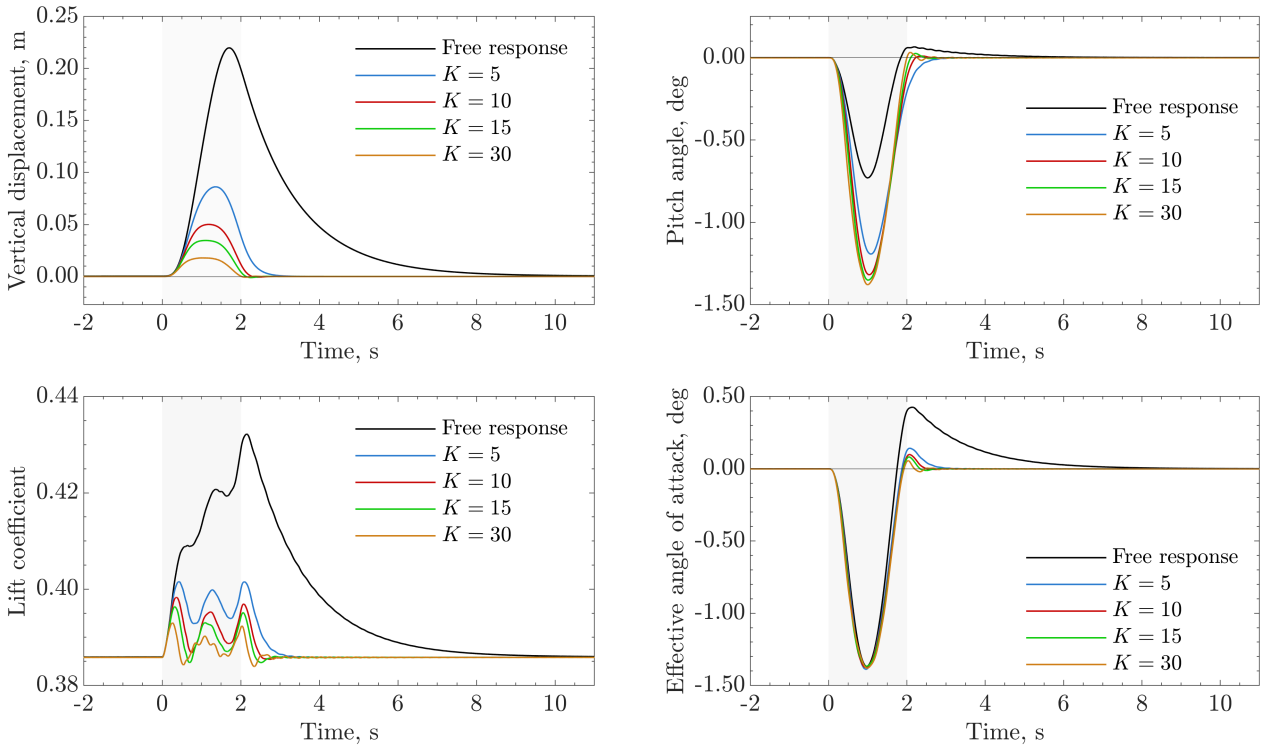

Fig. 7 Airfoil response to a frontal gust ($G = 0.25$, $f_g = 0.5$ Hz) under the action of the controller.

model, nevertheless, permits us to analyse the airfoil response in the first phase and to study the possibility of implementing a proportional pitch controller.

Figure 9 shows the airfoil response under the action of the pitch controller for different K values. Noticing once more the similarities between the effective angle of attack and the lift coefficient evolution, it was found that the lift coefficient can be approximated as $2\pi \times \alpha_{\text{eff}} + C_{L0}$. Being in a combined pitch-plunge motion, this is the lift that would correspond to a static case with an incidence equal to α_{eff}. We plot in Fig. 9 the comparison between the lift coefficient and the α_{eff}-based approximation.

In both gust cases, the time to reach the initial velocity is highly reduced no matter the controller constant used. The benefit of a high K value lies in the reduction of the maximum displacement.

The controller introduces a pitch moment as the airfoil increases its altitude. This means that the MAV will tend to decrease its pitch angle to reduce the upwards force generated by the gust. For the controlled response, the pitch angle is no longer a minor component of the effective angle of attack. In fact, the pitch reaches values between 6° and 14°. Considering the reduction in vertical velocity (and thus in the plunge-induced angle), the high pitch angle introduced is able to compensate for the gust-induced angle by "facing" the gust direction. As we increase the controller constant, the airfoil tends to align with the effective wind direction.

It can be noticed that there are some points at which the static approximation fails. To understand the reason, the flow features are discussed and related to the corresponding lift curves and and predictions. Figure 10 shows the velocity flowfield for different time instants for the uncontrolled $GR = 0.25$, $f_g = 0.5$ Hz case. The laminar separation bubble (LSB) can be observed in the scenes by looking at the white velocity area. The sequence shows that the LSB moves upstream when the lift increases, and downstream when it decreases. Akhlaghi et al. showed experimentally that, in a cyclic pitch-plunge motion, the LSB moves upstream when the effective angle of attack and the lift coefficient increase [15], a behaviour that is present in the vertical gust response.

In a combined pitch-plunge motion, the aerodynamic characteristics, including the LSB and the lift coefficient, depend not only on α_{eff} but on the airfoil movement and the α_{eff} sense of change. The lift coefficient becomes a multiple-valued function of the effective angle of attack [16]. In the lift coefficient hysteresis loops, the curve encircles the static lift values, forming a cycle in which each angle of attack corresponds to more than a single C_L value.

The increase and decrease in the effective angle of attack in the gust response may be analogous to a combined pitch-plunge motion where aerodynamic hysteresis appears. In that case, near the effective angle of attack extrema, we can expect the static approximation to fail. This approach is of higher accuracy after the gust duration, when the airfoil descends under the influence of the vertical spring of the structural model and no high vertical or angular accelerations appear.

C. Transverse gusts

Transverse gusts affect the stream-normal velocity and cause a vertical velocity. Their opposite contributions and the pitch angle are considered to obtain α_{eff} (at the leading edge):

$$\alpha_{\text{eff}} = \alpha + \alpha_{\text{pl}} + \alpha_{\text{gust}} = \alpha + \arctan\left(\frac{-\dot{y}(t)}{U_\infty}\right) + \arctan\left(\frac{v_s(t,0)}{U_\infty}\right)$$

A more in-depth study of the free response to transverse gusts has been carried out, analysing the effect of both the gust ratio and width.

To study the controller action, two gust cases with a sine-squared profile have been studied: a moderate-intensity gust of $GR = 0.25$ and $W = 15c$ and a less intense but smaller gust of $GR = 0.1$ and $W = 5c$. The airfoil response is analysed for five different control cases: the free (uncontrolled) response and four controlled responses with K ranging from 5 to 30.

The airfoil response to the transverse gusts can be divided into two main parts. The first one is a transitional phase for α_{eff} and C_L caused by the sudden perturbation of the gust, when, as a result, the airfoil increases its flight level. The shape of the curves in this phase depends strongly on the case studied

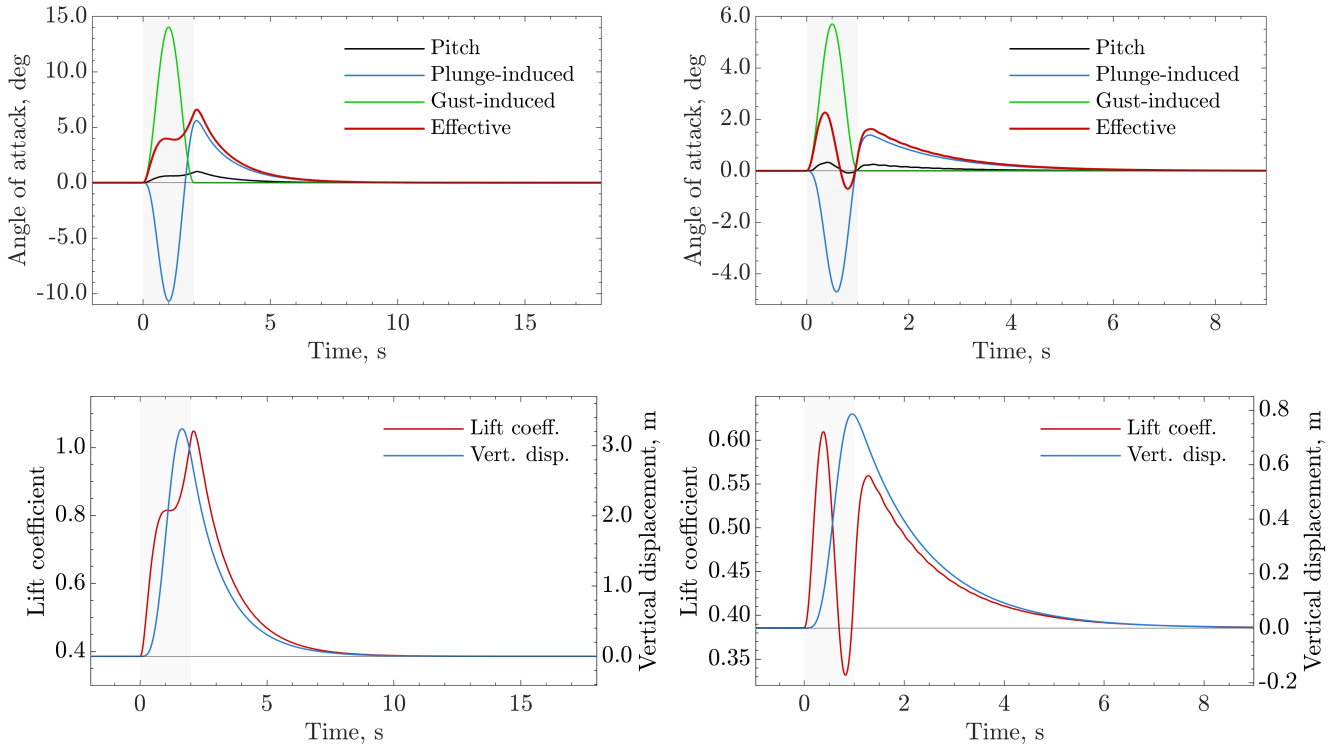

(a) GR = 0.25, f_g = 0.5 Hz. **(b) GR = 0.1, f_g = 1 Hz.**

Fig. 8 Airfoil response to two vertical gust cases.

and, therefore, unlike the vertical gusts, we cannot extract their general shape. After a certain period of time (which depends on the case studied), the lift coefficient and the effective angle of attack return to their initial value oscillating with a sinusoidal shape of a progressively decreasing amplitude and a constant period. This trend can be found in all the cases studied. The altitude maximum is reached shortly after the beginning of this phase, so an alternative division between the ascending and descending stages (as we did for frontal and vertical gusts) can be assumed.

To illustrate the transitional phase, we plot in Fig. 11 the evolution of the effective angle of attack and its components for the first seconds of the response of two gust cases. All the transverse gusts have been analysed using the convective time, which represents the number of chords travelled by the gust and is defined as:

$$t^* = \frac{U_\infty t}{c}$$

In Fig. 11, it can be seen that the gust ratio produces the same gust-induced angle in both cases.

In the case of the smaller gust width, a more sudden disturbance occurs, which causes the influence of the airfoil velocity to become noticeable once the gust has passed the airfoil, so that the first peak of the effective angle of attack is almost entirely due to the influence of the velocity profile of the gust. This is not the case for the higher width case, where the first peak of α_{eff} is smaller. However, we see that in this case the end of the transient phase is reached with higher amplitude oscillations.

Figures 12 and 13 show the effect of the gust ratio and the width in the airfoil response. The oscillation in the angle of attack leads to an oscillation in the lift coefficient. The vertical displacement increases until $t^* \sim 30$ approximately, when it reaches its maximum value. After that, the airfoil descends more slowly until $t^* \sim 600$, when the airfoil is at the initial position. The shape of the vertical displacement curve is similar to the one obtained for vertical gusts. The response shows small oscillation around the general trend explained, due to the oscillation present in the angle of attack and lift responses.

The GR influences the lift peak coefficients but not the oscillating period. For both the C_L and the vertical displacement curves, a linear relation can be found between the GR and the airfoil response. The gust width has a non linear relation with the height and lift coefficient responses. Figure 14a shows the variation of the peak C_L with the width for different GR. The peak lift coefficient increases with W until reaching $W = 10c$. At this point, the maximum peak is reached. For higher width, the peak CL remains constant and is even reduced. In the figure, the uniform distribution between the points of different GR for all the widths evinces the trends stated before.

Interestingly enough, the trends observed match the experimental results obtained by Badrya et al.[13], a study of a fixed flat plate at different incidences subjected to transverse gusts at Re $\sim$ 20000. Badrya et al. observed that, for an inceidence of 0°, a gust width of $6c$ produces indeed a maximum peak C_L, point from which this value is constant independent from W.

Another study by Biler and Jones showed that the lift coefficient evolution could be approximated using the effective angle of attack at the leading edge [6]. This approximation is the one discussed for frontal and vertical gusts: $2\pi \times \alpha_{\text{eff}} + C_{L0}$. Figure 14b shows that this approximation is only valid after the transitional phase. Even where the approximation can be used, we find the effect of the combined pitch-plunge motion found in vertical gusts, causing a deviation between the curves at the local lift extrema.

Figure 15 shows the effect of the controller constant on the airfoil response. The pitch controller reduces the maximum displacement and reduces the relaxation time. The vertical displacement effect is not as noticeable as for vertical or frontal gusts. The time to return to the initial position is reduced as we increase the K value except for K=30, where the relaxation time is higher than the rest of control cases. An excessive K value can be counterproductive in terms of relaxation time. The controller acts mainly on the first incidence cycles, increasing the pitch oscillation amplitude. This suggests that first lift, pitch and effective angle of attack oscillations, i.e. the most immediate response, determine the airfoil displacement response.

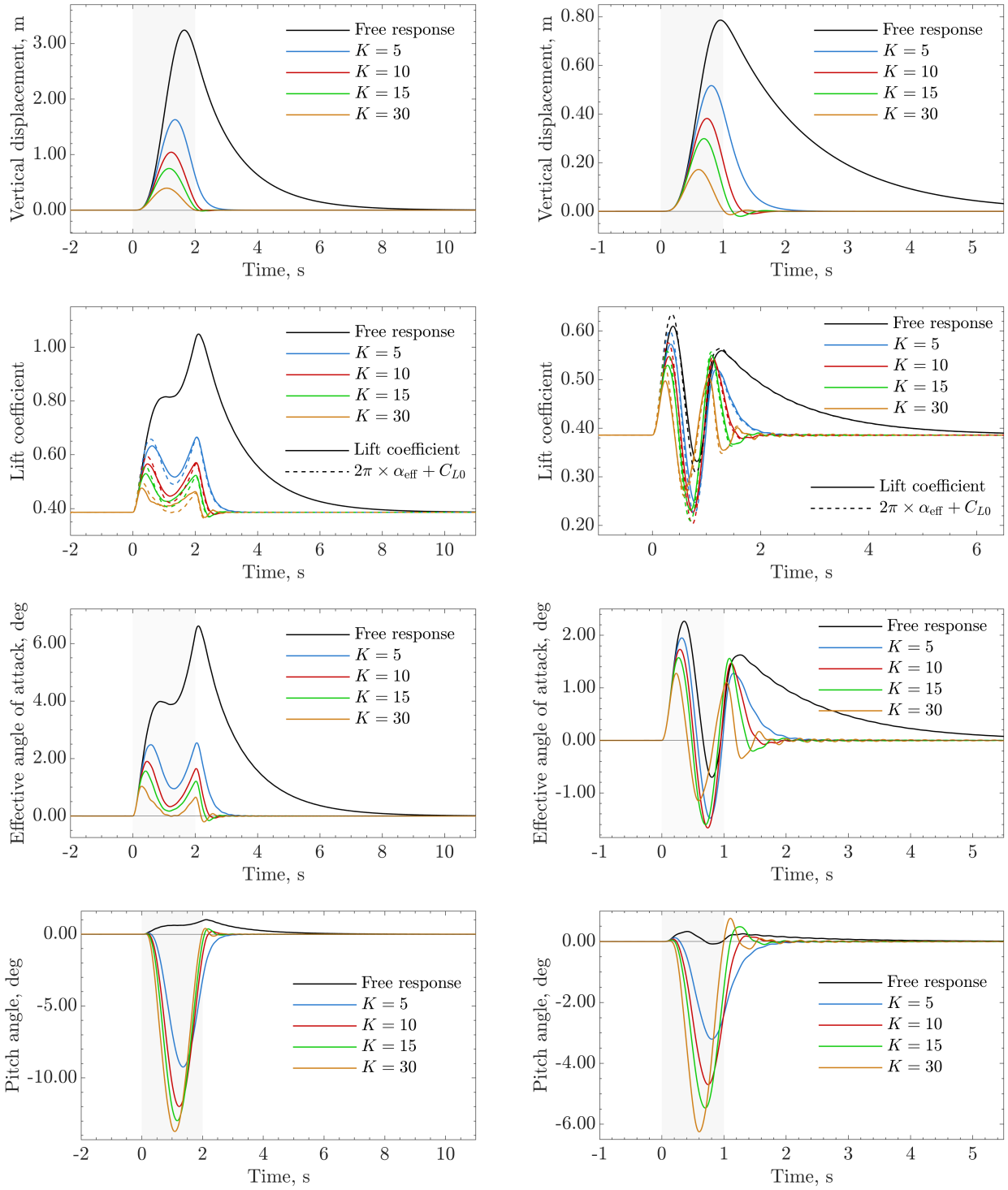

(a) GR = 0.25, f_g = 0.5 Hz. **(b) GR = 0.1, f_g = 1 Hz.**

Fig. 9 Airfoil response to two vertical gust cases under the action of a proportional controller.

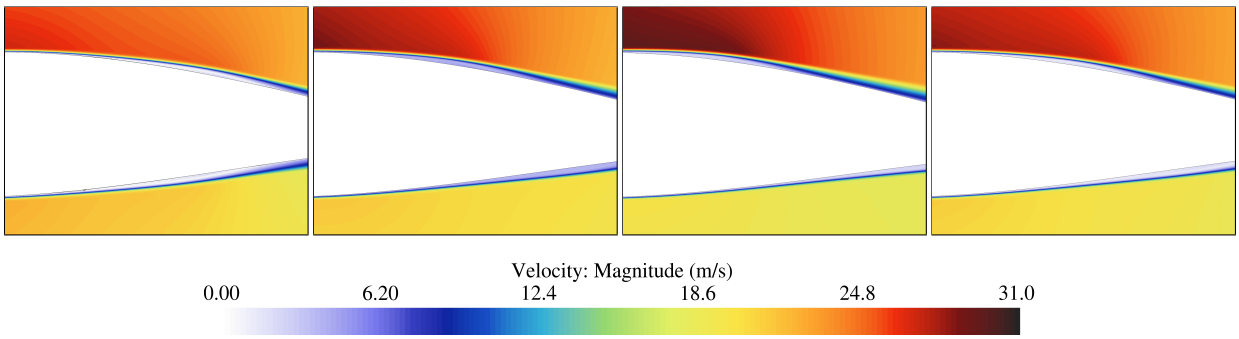

Fig. 10 Velocity scenes showing the LSB movement. Detail of the airfoil between 0.36c and 0.72c.

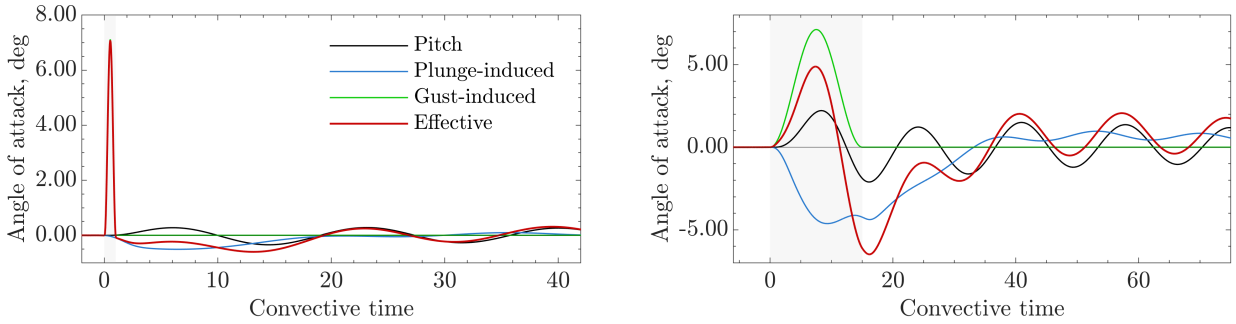

Fig. 11 Effective angle of attack components for $W = 5c$, $GR = 0.1$ (right), $W = 15c$, $GR = 0.1$ (left).

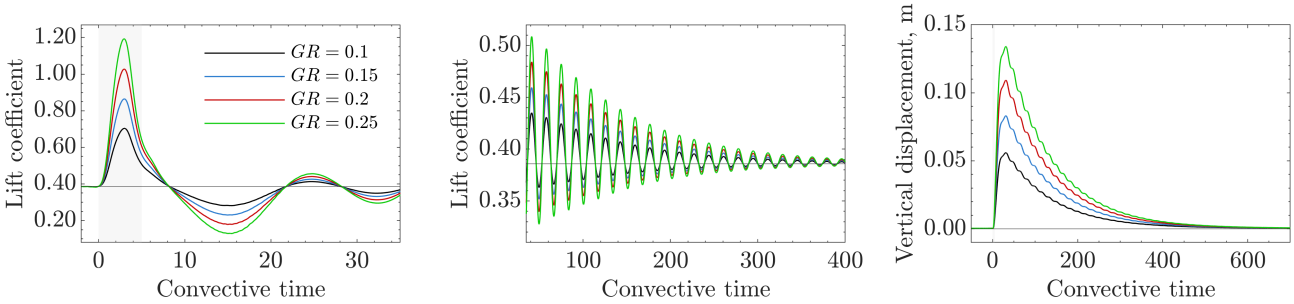

Fig. 12 Effect of the transverse gust ratio on the airfoil response for $W = 5c$.

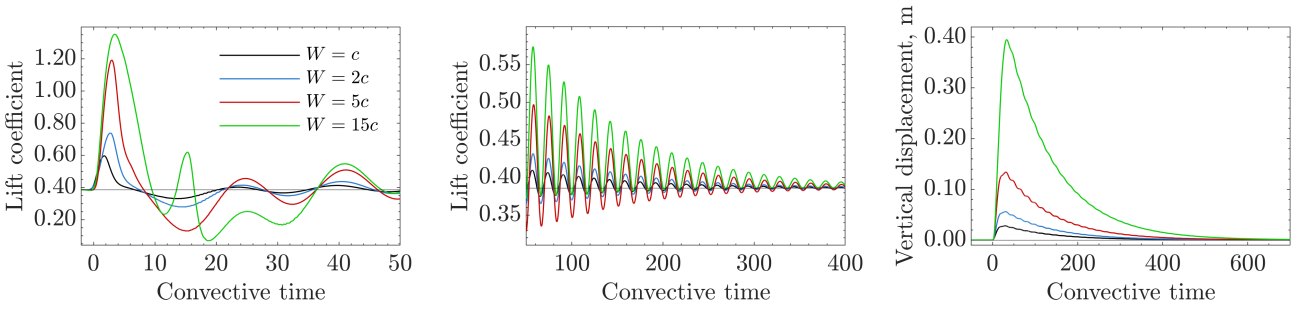

Fig. 13 Effect of the width of the transverse gust on the airfoil response for $GR = 0.25c$.

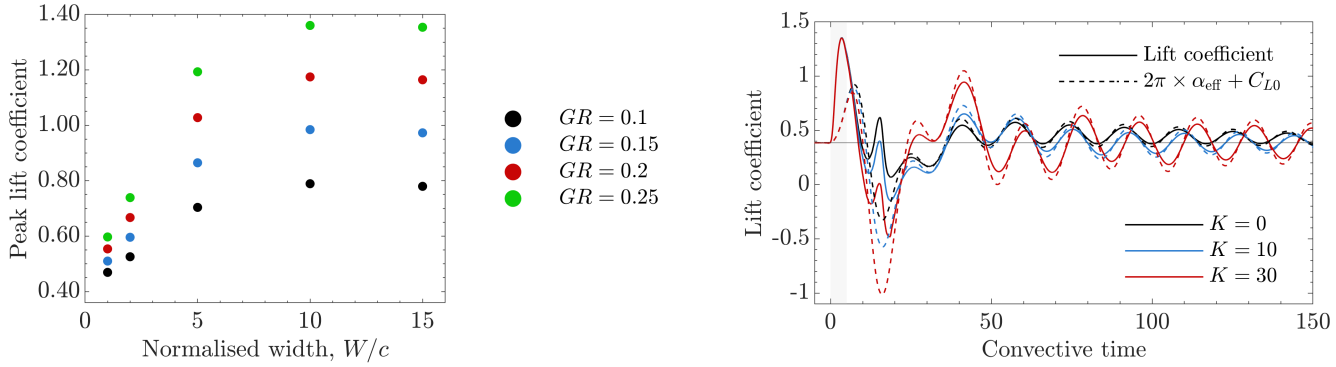

(a) Peak C_L as a function of W/c for different GR. **(b) Lift coefficient approximation using α_{eff} (GR=0.25,W=15c).**

Fig. 14 Transverse gust analysis as performed by Badrya et al.[6, 13].

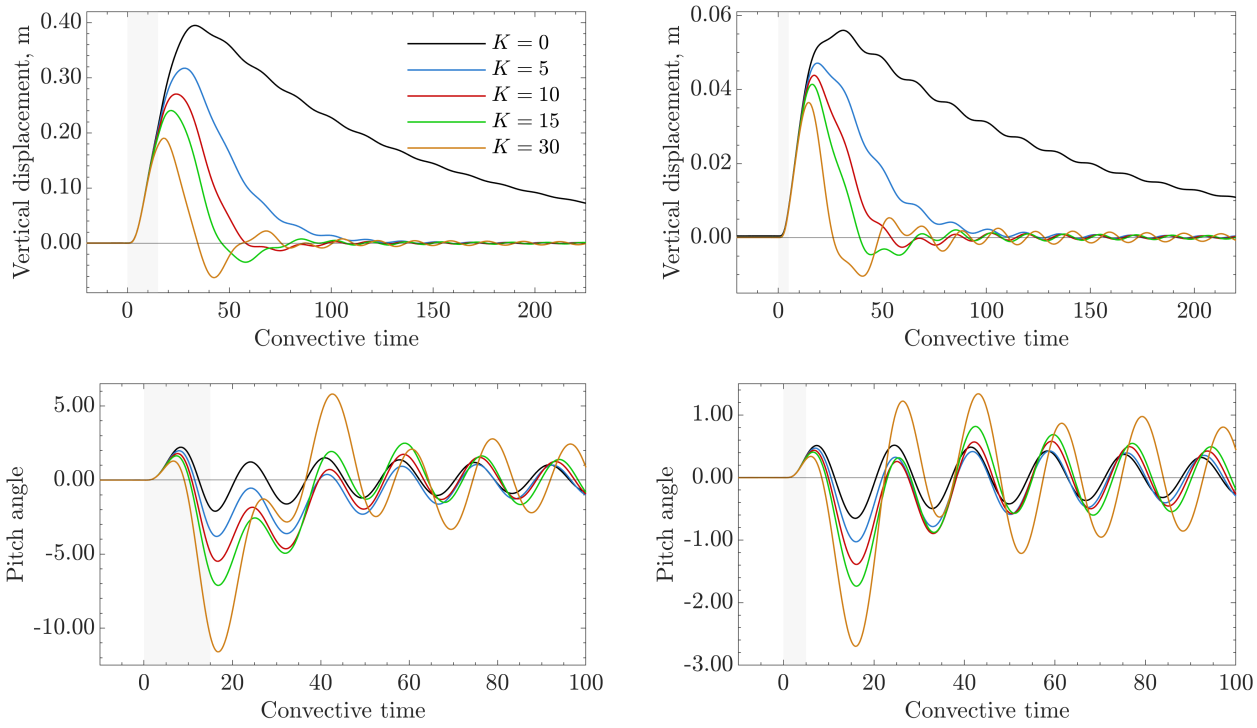

(a) $GR = 0.25$, $W = 15c$. **(b) $GR = 0.1$, $W = 5c$.**

Fig. 15 Airfoil response to two transverse gust cases under the action of a proportional controller.

V. Conclusion

In this paper, a numerical framework to simulate an airfoil response to different types of gusts that enables to simulate the action of a controller has been developed, tested and compared with existing studies for various gust and control cases.

We have devised a user-friendly methodology in a commercial software that permits to implement easily pitch controllers. This work uses a simple proportional controller, but more complicated may also be implemented with slight modification.

Most of the parameters of the simulations can be changed, like the spring constants, the inertia and centre of mass of the airfoil, the gust intensity, duration or width, making it possible to perform multiple parametric studies. Nevertheless, there are other parameters such as the mass, the moment M_0, the airfoil chord or the fluid cruise conditions which need from various preliminary simulations to be changed. Changing the simulated airfoil or the freestream velocity, for instance, modifies the lift in cruise, and as thus either the mass or the initial pitch angle need to be redefined accordingly to ensure cruise stability.

The framework allows to broaden the type of study. For instance, with little change, we could use the setup to perform aeroelastic analyses. Moreover, a potential study using the configuration in this paper could focus on the diverse multidisciplinary areas involved: fluid dynamics, automatic control, structural dynamics, etc.

This study focused on two great areas: the possibility of applying a proportional law to a UAV or a MAV and the airfoil gust response.

The proportional output-feedback strategy has shown good results when damping the gust response. The strategy of the controller is to apply a negative pitch when moving upwards, counteracting the vertical velocity and, in the case of vertical and transverse gusts, facing the effective wind direction. As a results, high pitch angles and pitch rates are obtained. Therefore, this strategy seems only suitable for vehicles such as UAV and MAV. A study for a specific air vehicle application should consider the maximum attainable K value. The $K = 30$ value, for example, may not be realistic for all the cases.

The controller showed a high reduction in the time to reach the equilibrium position for all the studied cases, returning in some cases before one half of the gust duration. Increasing the K value had more impact on the maximum displacement than on the relaxation time. In an application where the main objective is to minimise the return time to the original position and the reduction in maximum displacement is secondary, a lower K value might fulfil the requirements reducing the controller mechanism mass and complexity with respect to a higher one. An excessive controller constant can be counterproductive for transverse gusts.

Regarding the gust response, it was observed that, whereas frontal gusts induce vertical velocity and a negative effective angle of attack, vertical and transverse gusts tend to increase it, since the vertical velocity induced angle does not compensate for the upwards gust velocity induced angle.

Frontal and vertical gust responses were divided in two stages: the ascending and the descending phase. The maximum height, which marks the stage change, occurs before the end of the wind gust. It was observed that a lift coefficient local maximum was reached in the second phase. Other lift coefficient extrema appear in the first phase, as a result of the different contributions to the airfoil dynamics, which were analysed for the different gust types studied. Transverse gusts are divided in two different stages: one transitional and case-dependent phase followed by amplitude-descending oscillations around the initial value.

For frontal gusts, the gust response was attributed to two coupled components: the effective angle of attack and the velocity increase contributions. The interaction between these two generates a lift coefficient curve with three local maxima and two local minima. For vertical gusts, the α_{eff} curve has a characteristic shape with two local maxima with a local minimum in between. This shape is generated by a positive gust-induced profile and a shifted negative plunge-induced angle with a similar sinusoidal shape. For transverse gusts, the transitional phase appears to determine the displacement response.

By analysing both the free and controlled cases, a clear relation between the lift coefficient and the effective angle of

attack was found for vertical gusts. The lift coefficient could be approximated by $2\pi \times \alpha_{\text{eff}} + C_{L,0}$. This approximation failed in the curve extrema. The deviation was attributed to aerodynamics hysteresis. By means of flow visualisations, the movement of the airfoil was likened to a pitch-plunge motion where the aerodynamic characteristics depend on the airfoil motion and cannot be calculated with a static approximation. This approximation is also valid when the airfoil only after the transitional phase in a transverse gust encounter.

The peak lift coefficient in transverse gusts shows a characteristic evolution with the normalised gust width that was also found in previous experimental work by Badrya et al., a study performed at a much lower Re and with a fixed flat plate.

This article provides a versatile loop to gust response simulation and is a first step to link previous experimental studies with fixed airfoils and analytic models to the actual aircraft gust response dynamics. The dynamics simulations main limitation is the structural model. The implemented model influences how the airfoil interacts with the velocity perturbations and returns to its original position. We cannot ensure that the model represents with fidelity the actual aircraft dynamics, especially when the displacements are significant.

The project has the potential to examine airfoil-gust interaction in more depth. Next steps could include a study of the influence of the different vertical gust parameters in the airfoil response, to link it to the study carried out in the present work for transverse gusts. A larger data sample is needed to confirm the trends observed for transverse gusts, and a finer mesh should also be developed and use to simulate higher gust ratios and effective angles of attack.

In addition, the framework could be adapted to perform aeroelastic analyses, to study aircraft off-design conditions such as climbing or landing and to explore other control strategies like flap deflection. These points remain for future studies.

References

[1] Golubev, V. V., and Visbal, M. R., "Modeling MAV Response in Gusty Urban Environment," *International Journal of Micro Air Vehicles*, Vol. 4, No. 1, 2012, pp. 79–92. https://doi.org/10.1260/1756-8293.4.1.79.

[2] Xu, X., Zhu, X., Zhou, Z., and Fan, R., "Application of Active Flow Control Technique for Gust Load Alleviation," *Chinese Journal of Aeronautics*, Vol. 24, No. 4, 2011, pp. 410–416. https://doi.org/https://doi.org/10.1016/S1000-9361(11)60048-4.

[3] Gillebaart, T., Bernhammer, L. O., van Zuijlen, A. H., and van Kuik, G. A. M., "Active flap control on an aeroelastic wind turbine airfoil in gust conditions using both a CFD and an engineering model," *Journal of Physics: Conference Series*, Vol. 524, 2014, p. 012060. https://doi.org/10.1088/1742-6596/524/1/012060.

[4] Li, Y., and Qin, N., "Airfoil gust load alleviation by circulation control," *Aerospace Science and Technology*, Vol. 98, 2020, p. 105622. https://doi.org/https://doi.org/10.1016/j.ast.2019.105622.

[5] Sedky, G., Lagor, F. D., and Jones, A., "Unsteady aerodynamics of lift regulation during a transverse gust encounter," *Phys. Rev. Fluids*, Vol. 5, 2020, p. 074701. https://doi.org/10.1103/PhysRevFluids.5.074701.

[6] Biler, H., and Jones, A. R., "Force prediction during transverse and vortex gust encounters," *AIAA Scitech 2020 Forum*, 2020. https://doi.org/10.2514/6.2020-0081.

[7] Biler, H., Badrya, C., and Jones, A. R., "Experimental and Computational Investigation of Transverse Gust Encounters," *AIAA Journal*, Vol. 57, No. 11, 2019, pp. 4608–4622. https://doi.org/10.2514/1.J057646.

[8] Behal, A., Marzocca, P., Rao, V. M., and Gnann, A., "Nonlinear Adaptive Control of an Aeroelastic Two-Dimensional Lifting Surface," *Journal of Guidance, Control, and Dynamics*, Vol. 29, No. 2, 2006, pp. 382–390. https://doi.org/10.2514/1.14011.

[9] Xu, X., and Lagor, F. D., "Optimal Pitching in a Transverse Gust Encounter Using a Modified Goman-Khrabrov Model," *AIAA AVIATION 2021 FORUM*, 2021. https://doi.org/10.2514/6.2021-2937.

[10] Berci, M., Mascetti, S., Incognito, A., Gaskell, P., and Toropov, V., "Gust response of a typical section via CFD and analytical solutions," *Proceedings of the V European Conference on Computational Fluid Dynamics ECCOMAS CFD 2010*, edited by J. C. F. Pereira and J. M. C. Sequeira, Lisbon, Portugal, 14-17 Jun 2010.

[11] Jost, E., Lutz, T., and Krämer, E., "A Parametric CFD Study of Morphing Trailing Edge Flaps Applied on a 10 MW Offshore Wind Turbine," *Energy Procedia*, Vol. 94, 2016, pp. 53–60. https://doi.org/https://doi.org/10.1016/j.egypro.2016.09.192, 13th Deep Sea Offshore Wind RD Conference, EERA DeepWind'2016.

[12] Wales, C., Jones, D., and Gaitonde, A., "Prescribed Velocity Method for Simulation of Aerofoil Gust Responses," *Journal of Aircraft*, Vol. 52, No. 1, 2015, pp. 64–76. https://doi.org/10.2514/1.C032597.

[13] Badrya, C., Biler, H., Jones, A. R., and Baeder, J. D., "Effect of Gust Width on Flat-Plate Response in Large Transverse Gust," *AIAA Journal*, Vol. 59, No. 1, 2021, pp. 49–64. https://doi.org/10.2514/1.J059678.

[14] Kesarwani, A., Sundararaman, A., Jain, R., and Galal, M., "Transitional boundary layer on a pitching-plunging airfoil," *ISAE-SUPAERO*, 2021.

[15] Akhlaghi, H., Soltani, M.-R., and Maghrebi, M.-J., "Transitional boundary layer study over an airfoil in combined pitch-plunge motions," *Aerospace Science and Technology*, Vol. 98, 2020, p. 105694. https://doi.org/https://doi.org/10.1016/j.ast.2020.105694.

[16] Yang, Z., Igarashi, H., Martin, M., and Hu, H., "An Experimental Investigation on Aerodynamic Hysteresis of a Low-Reynolds Number Airfoil," *46th AIAA Aerospace Sciences Meeting and Exhibit*, 2008. https://doi.org/10.2514/6.2008-315, URL https://arc.aiaa.org/doi/abs/10.2514/6.2008-315.